inorganics

MDPI

Article

Heterostructure Based of Ti-TiO_2(NW)/rGO Hybrid Materials for Electrochemical Applications

Mina-Ionela Morariu (Popescu) [1,2], Mircea Nicolaescu [1], Corina Orha [1], Carmen Lăzău [1], Narcis Duteanu [2,*] and Cornelia Bandas [1,*]

[1] Condensed Matter Department, National Institute for Research and Development in Electrochemistry and Condensed Matter, 300224 Timisoara, Romania; mina.popescu@student.upt.ro (M.-I.M.); nicolaescu.mircea13@yahoo.com (M.N.); orha.corina@gmail.com (C.O.); carmen.lazau@gmail.com (C.L.)

[2] Department of Applied Chemistry and Engineering of Inorganic Compounds and Environment, Politehnica University of Timisoara, 300223 Timisoara, Romania

* Correspondence: narcis.duteanu@upt.ro (N.D.); cornelia.bandas@gmail.com (C.B.)

Abstract: This study investigated a hybrid electrode based on titanium/titanium dioxide nanowires/reduced graphene oxide (Ti-TiO_2(NW)/rGO) that was developed in two stages. The Ti-TiO_2(NW)/rGO was obtained by hydrothermal treatment in a mixed solution of H_2O_2 and melamine for Ti-TiO_2 support, followed by a simple spin-coating deposition method and thermal oxidation in a controlled atmosphere of nitrogen gas (99%). The as-prepared structures of electrodes were characterized using ultraviolet-visible spectroscopy (UV-Vis), X-ray diffraction (XRD), Raman spectroscopy, and scanning electron microscopy (SEM). In addition, the electrochemical behavior was assessed by cyclic voltammetry (CV) in a 1M HNO_3-supporting electrolyte and in the presence of 4 mM $K_4Fe(CN)_6$ $3H_2O$ to determine the electroactive surface area and apparent diffusion coefficient of the hybrid electrode. The development of the Ti-TiO_2(NW)/rGO hybrid electrode provides a sensitive method for photo-electrooxidation of doxorubicin due to exploiting the synergistic and remarkable properties of the nanowires of TiO_2 and of reduced graphene oxide (rGO) layer on the electrode surface.

Keywords: reduced graphene oxide; titanium dioxide nanowire; doxorubicin; electrooxidation; photo-electrooxidation

check for updates

Academic Editor: Huaiyu Shao

Received: 19 December 2024
Revised: 17 January 2025
Accepted: 19 January 2025
Published: 22 January 2025

Citation: Morariu, M.-I.; Nicolaescu, M.; Orha, C.; Lăzău, C.; Duteanu, N.; Bandas, C. Heterostructure Based of Ti-TiO_2(NW)/rGO Hybrid Materials for Electrochemical Applications. *Inorganics* **2025**, *13*, 31. https://doi.org/10.3390/inorganics13020031

Copyright: © 2025 by the authors. Licensee MDPI, Basel, Switzerland. This article is an open access article distributed under the terms and conditions of the Creative Commons Attribution (CC BY) license (https://creativecommons.org/licenses/by/4.0/).

1. Introduction

Nowadays, graphene-based electrodes are widely used and known as an excellent candidate in a wide range of applications (solar cells, LEDs, touch screens, batteries, and electrochemical sensors) due to the properties of graphene, such as chemical stability, excellent thermal, electrical, and mechanical properties, and high surface area. Particularly in the field of electrodes, graphene and its derivatives, such as graphene oxide (GO) and reduced graphene oxide (rGO), have been making a great impact in many areas of science and technology due to their remarkable physicochemical properties [1]. Until now, many reduction methods have been reported to obtain rGO sheets, such as chemical reagent reduction [2], thermal reduction [3], photochemical and electrochemical reduction [4], sonolytic reduction [5], photothermal reduction [6], microwave-assisted reduction [7], and electrochemical reduction [8]. Since graphene has a large electrochemical potential (2.5 V in 0.1 mM phosphate buffer solution), electrodes modified with graphene make it possible to detect molecules in a wide potential range. Further, the presence of edges and defects in

graphene contributes to a good electron transfer rate, which makes graphene a promising candidate for electrode materials [9].

A variety of GO-based hybrids with metal or metal oxide nanoparticles, such as Au, Ag, Pt, ZnO, TiO_2, and Fe_3O_4, have been developed, and the resultant nanomaterials showed excellent catalytic/photocatalytic properties compared with metal or metal oxide alone. Recently, numerous researchers have highlighted the use of graphene/metal oxide hybrid materials as catalysts and for water purification due to the synergic properties exhibited by the composites, such as higher absorptivity, conductivity, stability, and longevity [10]. Among them, a very promising composite was TiO_2/rGO, and many methods have been successfully adopted by researchers to synthesize this composite; thus, the hydrothermal method can be considered the easiest and most effective approach. Y. Liu prepared through a facile hydrothermal treatment nanocomposites based on TiO_2–RGO with different weight ratios of GO and Ti $(OH)_4$ in an ethanol-water solvent. The results showed that composites exhibited a layered structure with well-dispersed anatase TiO_2 on the surface of the reduced graphene oxide, and the photocatalytic activity was much higher than that of TiO_2 in the photodegradation of methyl orange under visible light irradiation [11]. N. Sun et al., in their studies, used a one-step hydrothermal method to prepare the TiO_2/reduced graphene oxide. The physical and chemical properties showed that TiO_2 nanoparticles, with a diameter of about 5 nm, were homogeneously dispersed over the rGO surface, and these materials have possessed potential application as high-performance renewable photocatalyst removal of toxic dyes from wastewater [12]. Besides the hydrothermal method, the combination of reduced graphene with TiO_2 can be realized through another classical method that creates a synergism of both the outstanding characters and functions of two components and leads to some additional novel properties. So, E. Cho et al. [13] reported the synthesis of TiO_2/graphene composite using a sol-gel method and observed that the composites exhibited high specific capacitance and good rate capability. Hence, the Graphene/TiO_2 electrode could be a promising candidate for supercapacitor applications. J. Guo et al. prepared TiO_2 particles and graphene via ultrasonication, achieving high performance in different potential applications, including optical, electrical, catalysis, sensors, and energy conversion devices [14]. Meng et al. reported the controllable synthesis of graphene-based TiO_2 nanocomposites via atomic layer deposition. These materials are promising candidates for numerous applications, such as lithium-ion batteries, solar cells, gas-sensing, and photocatalysis [15].

Using hybrid electrode materials based on graphene and metal oxide offers a promising approach to enhancing the electrochemical performance of metal oxides, as this strategy has several advantages. Superior to single-phase oxides, hybrid systems integrate several types of functional materials that can synergistically enhance the properties of each component, including electrical/ionic conductivity, electrochemical reactivity, and mechanical stability [16]. Metal oxides have received significant attention due to their diverse compositions and structures, flexible tunability, low cost, abundance, and environmental friendliness, making them ideal candidates for use as catalysts [17]. Until now, several conductive metal oxides have recently attracted considerable interest as alternative materials for conductive supports. For example, TiO_2, antimony-doped tin oxides, and tungsten oxides have been utilized as conductive supports with electrocatalysts for water electrolysis [18]. Among the various metal oxides used as supported catalysts on graphene, TiO_2 is the most attractive material due to its physicochemical properties, including good biocompatibility, strong adsorptive ability, high surface area, thermal stability, non-toxicity, and excellent electrical/electrochemical characteristics. The TiO_2/graphene hybrid electrode exhibits several synergistic effects from the interaction between the support and the catalyst. Thus, graphene, with its large surface area and superior electrical conductivity, facilitates

charge transfer between the two materials, thereby reducing charge recombination and enhancing the photocatalytic activity of TiO_2. Moreover, graphene can enhance the adsorption of pollutants on the catalyst surface, so the TiO_2/graphene hybrid electrodes have been employed in various applications, including air purification [19], degradation of pollutants in aqueous medium [20], Li-ion batteries [21], hydrogen production [22], and biosensors [23,24]. The photodegradation process of dye compounds as model-water pollutants is the most extensively studied in the presence of TiO_2/graphene-based hybrid materials. Additionally, various groups of pharmaceuticals as hazardous water contaminants have also been decomposed using TiO_2/graphene hybrids [25]. The presence of pharmaceutical compounds in water is one of the most serious global concerns because these substances cannot be removed through conventional wastewater treatment processes. When these compounds are released into the water supply without prior treatment, even in very low concentrations, they pose potential risks to the environment and human health [26].

Until now, many studies have reported that cytostatic drugs, including 5-fluorouracil, cyclophosphamide, ifosfamide, methotrexate, doxorubicin, epirubicin, and daunorubicin, exhibit poor biodegradability during the secondary stages of wastewater treatment processes [27,28]. Long exposure to low concentrations of doxorubicin (DOX) in water may increase the risk of developing long-term health issues. Furthermore, DOX in wastewater could compromise the effectiveness of conventional treatment methods, leading to the release of partially or fully untreated effluent into the environment [29]. Several conventional methods, including chlorination [30], ozonation [31], reverse osmosis [32], activated carbon adsorption [33], ultra-filtration [34], and electro-coagulation [35], have been applied to remove hospital pollutants from wastewater. However, these techniques have different drawbacks that make it difficult to achieve the desired wastewater treatment. In our previous studies, we tested the degradation and mineralization of DOX in water through electrooxidation using a new 3-D dimensionally stable anode, both as a single component and multi-component, together with capecitabine from the cytostatic class and humic acid from the natural organic matter class, in the absence and presence of activated carbon as a particulate electrode. The results showed a 52.75% TOC removal of DOX, and a synergic effect was observed when considering the kinetics aspects of all electrooxidation, sorption, and activated carbon-assisted electrooxidation processes [36,37]. Also, our team previously developed a titanium/TiO_2 mesoporous/reduced graphene oxide structure to construct a hybrid electrode, which was tested for detecting different concentrations of the DOX drug. The results revealed that the electrode had an enhanced electroactive surface area and electrocatalytic properties for DOX detection, opening up some perspectives for further enhancing the electroanalytical performance of the hybrid electrode [38]. Therefore, this research aimed to obtain a hybrid electrode based on titanium/titanium dioxide nanowires/reduced graphene oxide (Ti-TiO_2(NW)/rGO) in two stages, by hydrothermal treatment followed by spin-coating deposition methodology and tested for degradation of cytostatic pharmaceutical compound doxorubicin (DOX). The Ti-TiO_2(NW)/rGO electrode was morpho-structurally and electrochemically characterized and tested in the electrooxidation and photo-electrooxidation processes for DOX degradation.

2. Results and Discussion

2.1. Structural, Morphological and Electrochemical Characterization

Figure 1a presents the XRD patterns for Ti-TiO_2(NW) support, and Figure 1b compares the spectra for hybrid electrode Ti-TiO_2(NW)/rGO before and after deposition of the reduced graphene oxide layer. Therefore, in Figure 1a, the support compound Ti-TiO_2(NW) shows the presence of three phases of TiO_2 (anatase, rutile, and brookite). The presence of strong peaks recorded for the 2theta values of anatase (tetragonal structures): 25.68°,

38.39°, 48.79°, and 54.77°, corresponding to JCPDS references code 01-075-1537; 27.96°, 35.70°, 41.08°, and 55.65°, corresponding to JCPDS references code 01-082-0514 for rutile (tetragonal structures); 25.34°, 25.68°, 55.23°, and 70.43°, corresponding to JCPDS 00-028-1360 with orthorhombic structures for brookite. Hexagonal structures of Ti element were identified due to their prominent peaks at the specific 2theta values: 38.42°, 40.17°, 53.1°, 62.95°, and 70.66°, corresponding to the JCPDS reference code 00-044-1294. The crystallite sizes (D) of different polymorphs of TiO_2 were calculated using the most intense peak, following Debye–Scherrer's Equation (1) [39].

$$D = K\lambda/\beta \cos\theta \quad (1)$$

where D—crystallite size on the most intense pick, K—Scherrer's constant (0.89), λ—X-ray wavelength, θ—Bragg diffraction angle, β—FWHM of the diffraction peak

The crystallite size of TiO_2 anatase (101) was 14.5 nm, TiO_2 rutile (110) was 24.2 nm, and TiO_2 brookite (121) was 18.1 nm. Y. Yu and their team synthesized TiO_2 nanowires (TiO_2-NW) using a melamine template, demonstrating the formation mechanism. During the hydrothermal treatment of a Ti plate with melamine, hydrogen titanate ($H_2Ti_5O_{11}$) nanowires formed on the surface. Subsequent thermal treatment decomposed $H_2Ti_5O_{11}$ into TiO_2 while preserving the nanowire configuration. In their study, only anatase and rutile phases were synthesized, unlike our study, where structural analysis also identified the brookite phase. This additional phase from our work may enhance the catalytic properties due to the formation of multiple-phase junctions [40]. W. Guo investigated the morpho-structural changes in TiO_2 depending on pyrolysis temperature, showing that all TiO_2 polymorphic phases were formed at 650 °C [41]. So, in our study, we successfully evidenced the formation of all three polymorphic phases at a lower temperature (500 °C). This demonstrates that factors beyond temperature, such as hydrothermal parameters like the degree of fullness and the diameter of the autoclave, also significantly influence phase formation.

Moreover, as shown in Figure 1b, the presence of an rGO peak is not clearly evidenced, probably because of the thin layer of GO deposited by the spin-coating method and because the (101) peak of TiO_2 anatase (melamine template) coincides with the peak of rGO that presents an intensity on the range 2theta = 20–30°. Also, the Ti-TiO_2(NW)/rGO hybrid structure presents a high intensity of the diffraction peaks from Ti foil (the basic support), and the diffraction plane reflects a thermal reduction from the GO to rGO layer [42]. Therefore, to identify the vibrational states of the as-developed hybrid electrode, Raman spectroscopy was performed (Figure 1c). The increasing value to 1.15 of the ratio I_D/I_G suggests the appearance of defects after the reduction process for the Ti-TiO_2(NW)/rGO hybrid structure, confirming the reduction of GO to rGO.

The absorption spectra of the Ti-TiO_2(NW) and Ti-TiO_2(NW)/rGO hybrid structures are reported in Figure 2 in the range of 400–600 nm. A strong absorption in the UV region is observed for both as-developed structures, attributed to the presence of TiO_2. As shown in Figure 2a, the corresponding wavelength for the Ti-TiO_2(NW) and Ti-TiO_2(NW)/rGO hybrid electrode was about 420 nm, and it is highlighted that the presence of the GO layer influences the optical properties of light absorption and increases the intensity of the absorbance. The increased absorbance in the UV region is determined by the interaction between the TiO_2 and rGO, according to S. Sheshmani et al. [43]. The Eg optical bandgap energy was calculated by Tauc plot [44], as presented in Figure 2b, and the estimated value of the Ti-TiO_2(NW)/rGO hybrid electrode was increased at 1.94 eV probably because of the rGO presence on the surface of the Ti-TiO_2(NW) electrode.

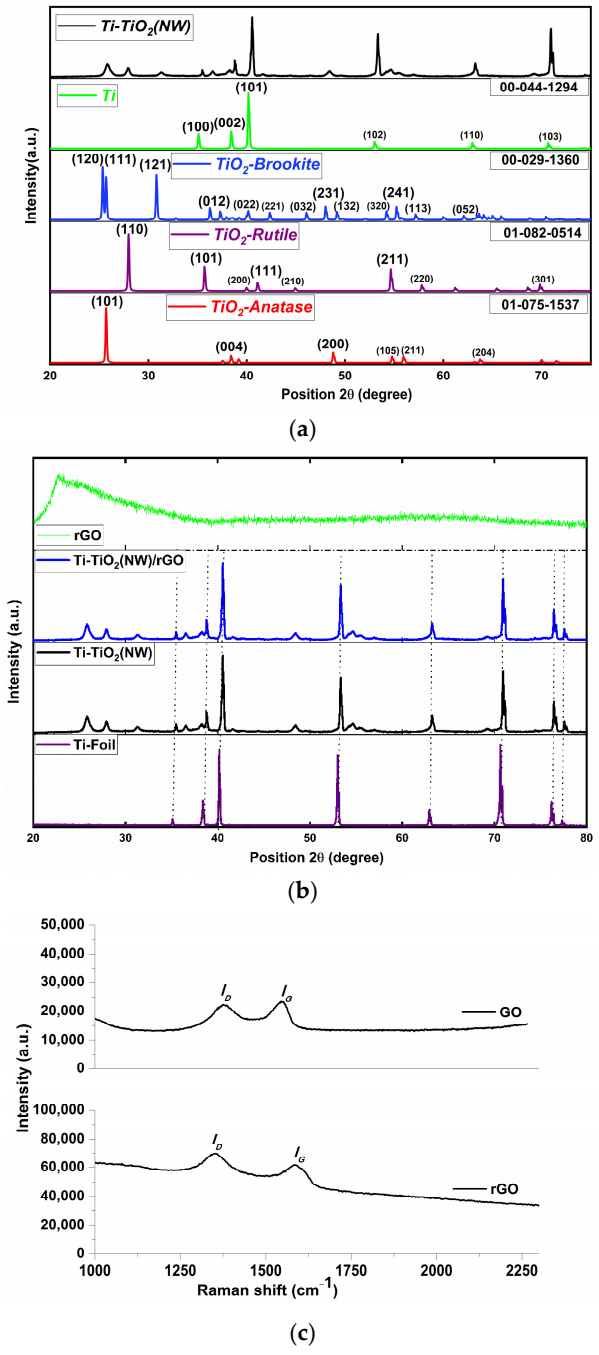
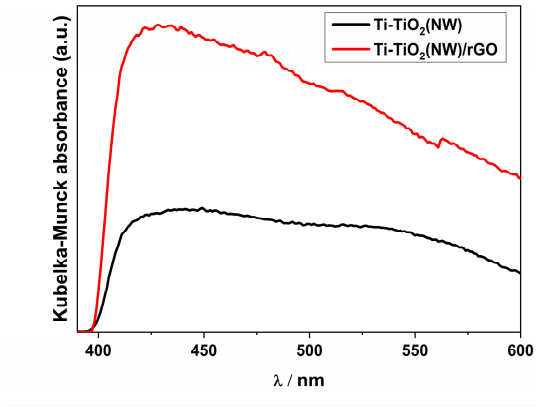
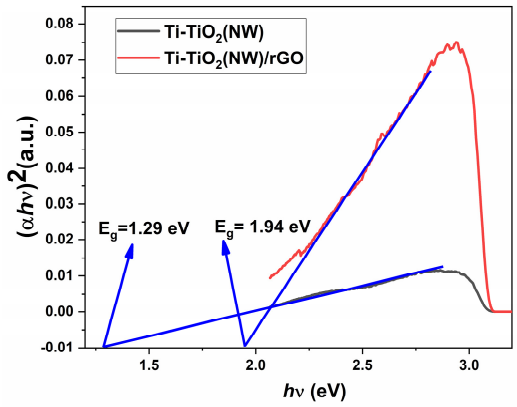


Figure 1. X-ray patterns for (**a**) as-synthesized structures of Ti-TiO_2(NW); (**b**) as-development hybrid electrode of Ti-TiO_2(NW)/rGO. Raman spectra of the hybrid electrode (**c**).

Figure 3 shows the SEM morphologies of the Ti-TiO_2(NW) and Ti-TiO_2(NW)/rGO hybrid electrodes. It can be observed in Figure 3a that the Ti foil presents a significant change in the morphology after the corrosion process and the hydrothermal treatment (72 h at 80 °C). The titanium foil surface was preferentially corroded, favoring the formation of channels on the surface so that the TiO_2 nanowires grew irregularly with a random orientation on the islands on the surface of the electrode. It was also found that the average thickness of the TiO_2 nanowires is 0.0548 µm (measured using ImageJ software Version 1.53t). In the case of the Ti-TiO_2(NW)/rGO structure (Figure 3b), even though channels form on the electrode surface following the corrosion process, the TiO_2 nanowires have formed island conglomerates. Thus, the uniform deposition of rGO on the electrode surface was evident.



(**a**)



(**b**)

Figure 2. Kubelka-Munck absorbance of the electrodes (**a**) and Band-gap calculation using the Tauc method (**b**).

The electrochemical characterization of the Ti-TiO_2(NW)/rGO hybrid electrode was assessed using the cyclic voltammetry method in the presence of 4 mM ferro/ferricyanide $K_3Fe(CN)_6$ $3H_2O$ redox couple as an electrochemical model of a reversible redox system. Figure 4 shows the cyclic voltammograms of 1 M KNO_3 supporting electrolyte in the presence of 4 mM $K_3Fe(CN)_6$ recorded for the tested Ti-TiO_2(NW)/rGO hybrid electrode at increasing potential scan rate from 0.025 to 0.3 V s^{-1}. The electroactive surface area of the Ti-TiO_2(NW)/rGO hybrid electrode and the apparent diffusion coefficient were calculated based on the Randles–Sevcik Equation (2) [45]:

$$Ip = 2.69 \times 10^5 AD^{1/2} n^{3/2} v^{1/2} C \quad (2)$$

where:

A—represents the geometric surface area of the sensor (cm^2)—0.8; n—represents the number of participating electrons in the reaction, equal to 1; D—represents the diffusion coefficient of the molecules in solution (cm^2 s^{-1})—4.52 cm^2 s^{-1}; C—is the molar concentration of $K_3Fe(CN)_6$ $3H_2O$ in the solution (i.e., 4 mM); and v—represents the scanning speed (V s^{-1}).

Based on the literature data, where Kenopka et al. [46] presented the theoretical diffusion coefficient value of 6.7 × 10^{-6} cm^2 s^{-1} reported for twin electrode thin-layer electrochemical cell, in our study for as-developed Ti-TiO_2(NW)/rGO hybrid electrode a higher diffusion about 4.5 × 10^{-5} cm^2 s^{-1} was exhibited. Due to the presence of rGO film

on the Ti-TiO_2(NW) electrode surface, the recorded electroactive surface area of 2.07 cm^2 was higher than the geometrical surface area of 0.8 cm^2.

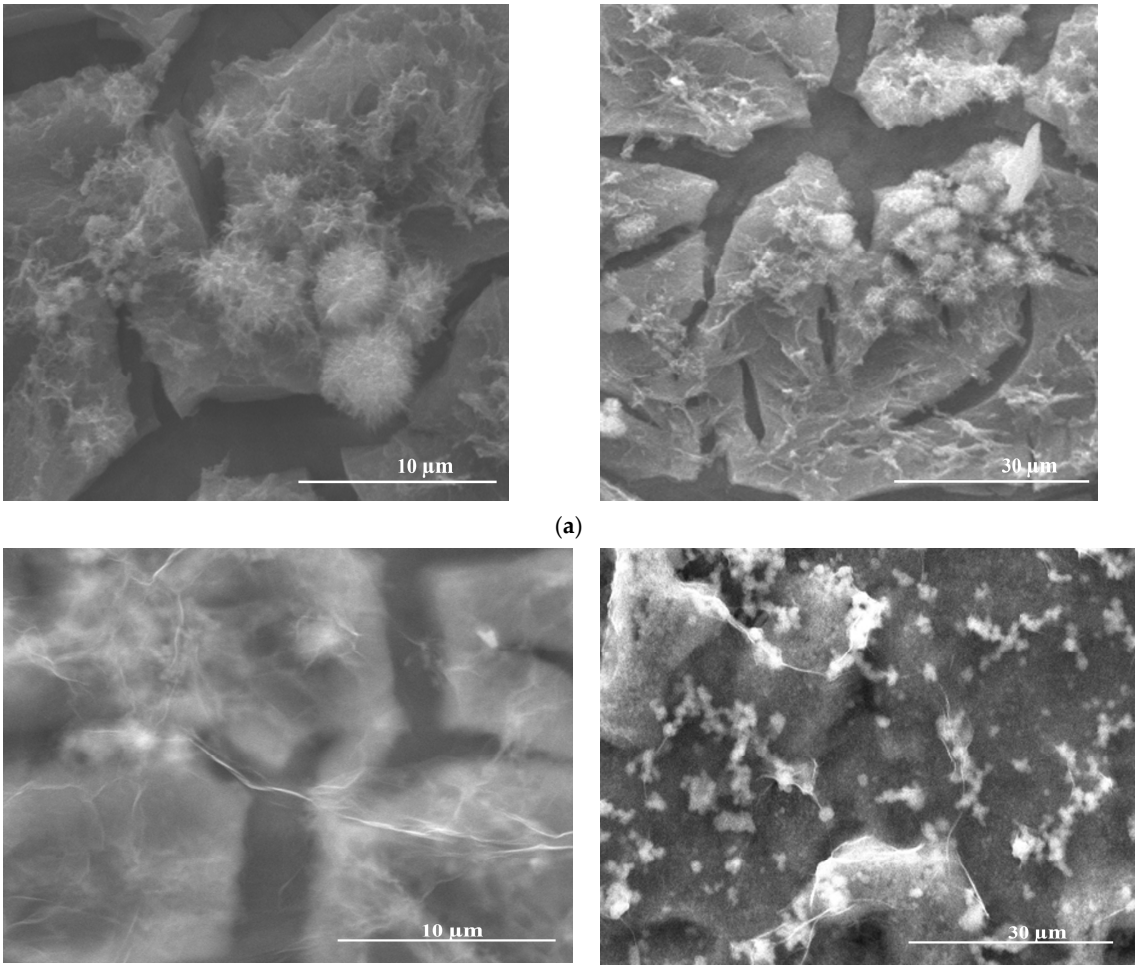
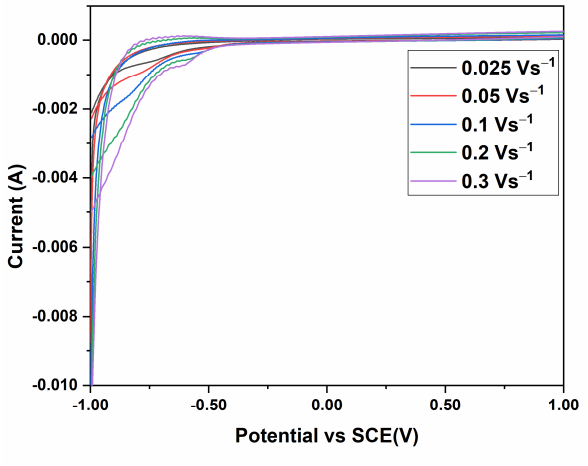
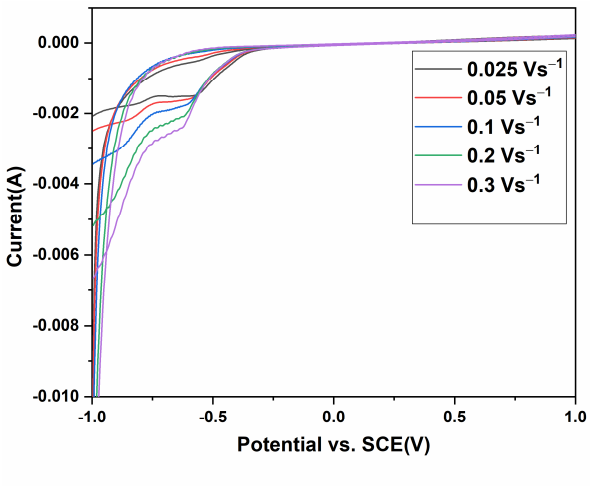


Figure 3. SEM morphologies for Ti-TiO_2(NW) electrode (**a**) and Ti-TiO_2(NW)/rGO hybrid electrode (**b**) at different magnifications.



(**a**)

Figure 4. *Cont.*



(**b**)

Figure 4. Cyclic voltammograms of 1 M KNO_3 supporting electrolyte (**a**) and in the presence of 4 mM $K_3Fe(CN)_6$ (**b**) for the Ti-TiO_2(NW)/rGO hybrid electrode.

2.2. Testing of the Ti-TiO_2(NW)/rGO Hybrid Electrode for DOX Degradation

The experiments were carried out by batch processes using an undivided cell of 1 dm^3 capacity, 2.5 mg L^{-1} DOX in 0.1 M NaCl as an electrolyte, without pH correction under constant temperature conditions (room temperature). The suspension was illuminated with a 6 W UV lamp emitting 254–365 nm wavelengths; the schematic representation is illustrated in Figure 5.

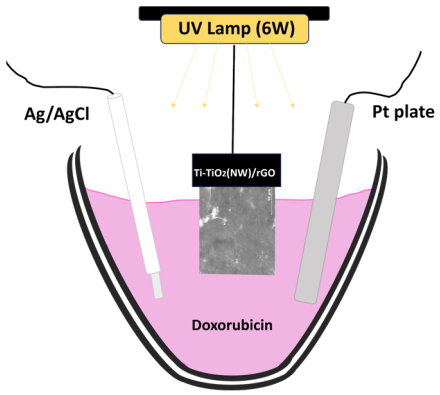
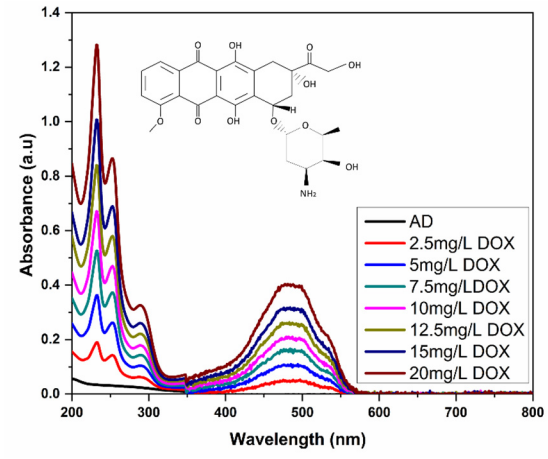
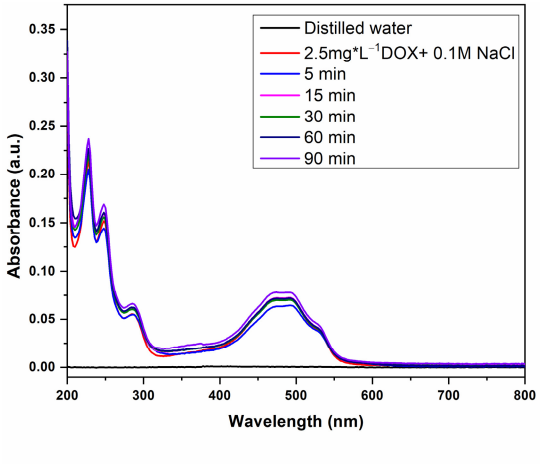


Figure 5. Schematic representation for testing the Ti-TiO_2(NW)/rGO using 0.1 M NaCl supporting electrolyte and 2.5 mg L^{-1} DOX.

In order to choose the optimal pollutant concentration for testing the hybrid electrode, with an effective surface of 0.5 × 0.8 cm^2, we realized an absorbance spectrum varying the doxorubicin concentration for 2.5, 5, 7.5, 10, 12.5, 15, and 20 mg L^{-1}. Due to the small surface of the electrode, it was established that the optimal concentration for degradation processes is 2.5 mg L^{-1} DOX. Also, for the electrooxidation and photo-electrooxidation processes, the initial concentration is one of the most important parameters for the degradation of compounds. As a contaminant with a lower concentration, access to the electrode surface, secondary products, and organic intermediates is easier [47]. Following the UV-Vis spectrum of DOX, the absorbance peaks were monitored at different wavelengths, being recorded at the values of A_{232}, A_{253}, A_{290}, and A_{486} nm, as presented in Figure 6a.



(**a**)



(**b**)

Figure 6. UV-VIS spectra for 2.5, 5, 7.5, 10, 12.5, 15, and 20 mg L^{-1} DOX (**a**); UV-VIS spectra for 2.5 mg L^{-1} DOX in 0.1 M NaCl supporting electrolyte and under UV irradiation (**b**).

The solution of 2.5 mg L^{-1} DOX in 0.1 M NaCl supporting electrolyte was tested for 90 min (Figure 6b) to verify the influence of UV irradiation on DOX degradation. Thus, it was observed that after irradiation with a 6 V UV lamp for 90 min without applying a current potential, the DOX solution did not change color, proving that during irradiation, the color remained unchanged (A_{486}). The emerging pollutant doxorubicin remains present in the solution. Therefore, it can be concluded that UV radiation is not responsible for the degradation of DOX. Since the supporting electrolyte plays an important role in pollutant degradation, we selected NaCl for our testing experiments. Because chlorine radicals and molecular chlorine are formed from the anodic oxidation of Cl^-, so this is the main oxidant produced during the electrooxidation and photo-electrooxidation of the DOX in an aqueous solution based on chlorine. Thus, NaCl-supporting electrolytes, compared to Na_2SO_4, produce a higher degree of acceleration of the doxorubicin degradation process [48]. Because the combination of rGO and TiO_2 is proven to play a synergistic effect and effectively improve the properties of the materials, the TiO_2 nanowires can effectively avoid agglomeration and shorten ion diffusion length during the electrochemical process [49].

Electrooxidation and photo-electrooxidation processes were performed using the classical three-electrode cell, consisting of Ti-TiO_2(NW), respectively, Ti-TiO_2(NW)/rGO as working electrodes, and an Ag/AgCl as reference electrode and a platinum counter elec-

trode. The electrooxidation process was carried out in 0.1 M NaCl supporting electrolytes for the degradation of 2.5 mg L^{-1} DOX using an applied potential of 7 V/SCE.

For the evaluation of the Ti-TiO_2(NW) and Ti-TiO_2(NW)/rGO electrode performances under the electrooxidation and photo-electrooxidation processes, UV-VIS spectra were recorded (Figure 7). Firstly, the Ti-TiO_2(NW) electrode was tested, and the UV-VIS evolution within the photo-electrooxidation and electrooxidation processes showed the DOX degradation efficiency after 90 min about 45%, respectively 37% (Figure 7a,b). In the case of Ti-TiO_2(NW)/rGO as a working electrode during the electrooxidation process, after 30 min, the electrode was saturated, and the degradation process of DOX was stopped. Also, as we proved in our previous paper [37], we emphasized that ozone, hydroxide radicals, and intermediate organics (Figure 7c) can be formed and can act as oxidizing agents during the photo-electrochemical process (Figure 7d) [37]. The Ti-TiO_2(NW)/rGO electrode's ability to degrade DOX is based on the synergistic interaction between rGO nanowires and TiO_2 (grown on melamine support), resulting in the production of strong oxidants (OH) on its surface. Therefore, after the photo-electrooxidation process, approximately a rate of 80% for DOX degradation was achieved (Figure 7d).

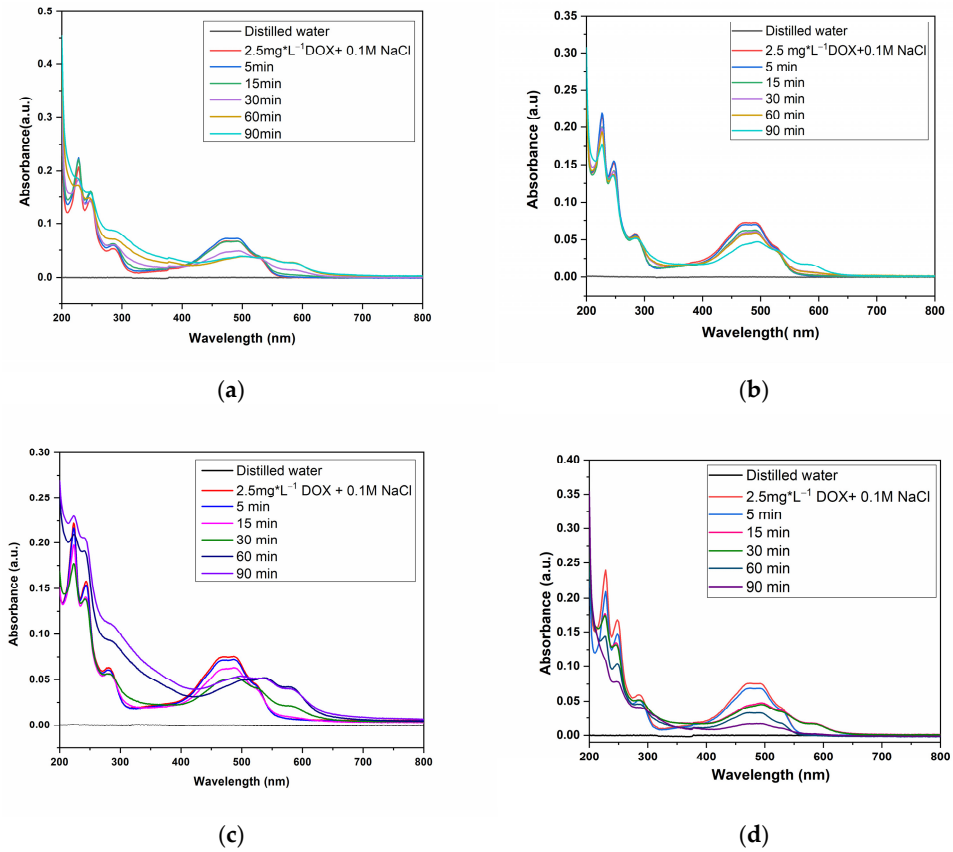


Figure 7. UV-spectra after the electrooxidation (**a**,**c**) and photo-electrooxidation (**b**,**d**) processes obtained for the Ti-TiO_2(NW) (**a**,**b**) and Ti-TiO_2(NW)/rGO (**c**,**d**).

The DOX degradation degree was calculated for absorbances at wavelength A_{486} and A_{253} nm according to Equation (3):

$$\eta = (C_{DOX,I} - C_{DOX,f})/C_{DOX,i} \times 100\ (\%) \quad (3)$$

where: $C_{DOX,i}$—represents the initial concentration at the wavelength of the absorbers A_{486} and A_{253}; $C_{DOX,f}$—represents the final concentration at the wavelength of the absorbers A_{486} and A_{253}. Therefore, using NaCl as electrolyte support and with the help of a UV

lamp and Ti-TiO_2(NW)/rGO as an electrochemical electrode demonstrated a superior DOX degradation.

In this study, the DOX degradation efficiency using the Ti-TiO_2(NW) and Ti-TiO_2(NW)/rGO electrodes was evaluated and compared separately in the electrooxidation and photo-electrooxidation processes (Figure 8). Figure 8a,b shows that using Ti-TiO_2(NW) supports the DOX degradation efficiency for η-A486, which was about 45% after 90 min within the photo-electrooxidation process, and only 20% for η-A253. Figure 8c,d shows that the kinetics of color removal by electrooxidation are significantly slower than those for photo-electrooxidation. The initial color A_{486} of DOX using a Ti-TiO_2(NW)/rGO electrode is reduced by 35% by the electrooxidation process (Figure 8c). Under UV irradiation and applied potential within the photo-electrooxidation process, an 80% degradation rate after 90 min of treatment was achieved (Figure 8d). UV irradiation produces free radicals that can oxidize organic compounds by affecting some electrooxidation process products.

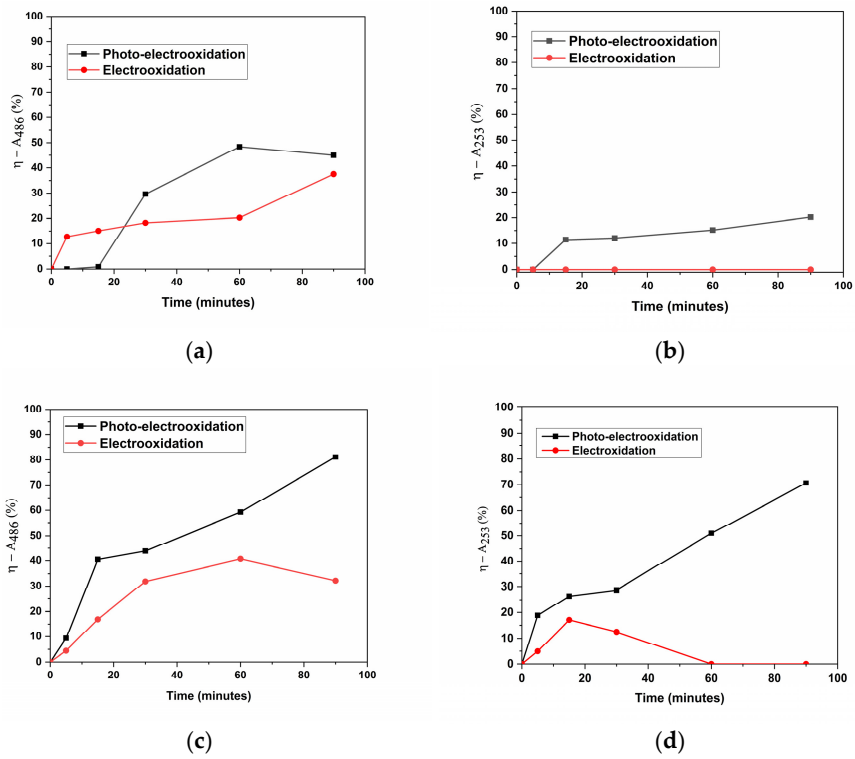


Figure 8. DOX degradation efficiency operated at 7 V/SCE and 2.5 mg L^{-1} DOX in 0.1 M NaCl supporting electrolyte for Ti-TiO_2(NW) (**a**,**b**) and Ti-TiO_2(NW)/rGO (**c**,**d**) electrodes.

Table 1 emphasizes different electrode types used for different DOX degradation processes. In our work, we highlighted the various synergistic effects resulting from the combination of TiO_2 nanowires and rGO. For example, graphene offers a large surface area, enhances the adsorption of organic pollutants on the electrode surface through π-π stacking, and its superior electrical conductivity reduces charge recombination, thereby improving the photo-electrooxidation activity of TiO_2.

Table 1. Different types of electrodes used for the DOX degradation process.

Materials	Type	Degradation Process	Removal Efficiency (%)	Concentration (mg L^{-1})	Time (min)	References
AuO-TiO_2@graphite	Graphite-Electrode	EO (electrooxidation)	100	1.25	40	[50]
Doxorubicin solution (+MOFs as photocatalysts)	Solution	Photodecomposition (in daylight-in the shade)	100	0.030	120	[51]
GO-CeO_2	Nanocomposites	Adsorption /Photodegradation	97	0.5 mM	120/240	[52]
Doxorubicin solution	Solution	Photodegradation	70	0.01	10.080	[53]
Fe-Ni NP's (bimetallic nanoparticles)	Powder	Chemisorptive exothermic pseudo-multilayes film-diffusion mineralisation	84	100	20	[54]
$BiFeO_3$	Powders	Photocatalysis	79	2	180	[55]
BDD-commercial electrode	Electrode	Electrooxidation	100	1.25	20	[56]
Ti-TiO_2(NW)/rGO	Electrode	Photo-electrooxidation	80	2.5	90	This work
Ti-TiO_2(NW)/rGO	Electrode	Electrooxidation	35	2.5	90	This work

3. Materials and Methods

3.1. Chemicals

Graphene oxide (4 mg/mL) dispersed in H_2O, titanium foil (thickness 0.25 mm, 99% purity), acetone, ethyl alcohol, melamine, hydrofluoric acid (HF), nitric acid (HNO_3), doxorubicin hydrochloride, and sodium chloride (NaCl) were purchased from Sigma-Aldrich Company (St. Louis, MO, USA).

3.2. Development of the Ti-TiO_2(NW)/rGO Electrode

The Ti-TiO_2(NW)/rGO hybrid structure was prepared in a two-stage schematic illustrated in Figure 9.

I. Achievement of Ti-TiO_2(NW) electrode: First, Ti-TiO_2(NW) electrode corrosion of the Ti foil was achieved and finally subjected to a hydrothermal treatment. Thus, Ti foil (effective area 1 × 1.2 cm^2) was cleaned in acetone, ethanol, and distilled water for 10 min in an ultrasonic bath. Afterward, the Ti foil was corroded by being treated in a mixed solution of HF: HNO_3: DW (2:3:6) for 10 min in order to remove the first layer of oxide (naturally formed on the surface of the Ti foil), and after that, the foil was rewashed in distilled water, ultra-sounded for 10 min, and dried in a vacuum at 60 °C. The growth of the TiO_2(NW) was done using chemical oxidation with melamine as a soft template in consistency with other studies [40]. Thus, the corroded Ti foil was placed in the autoclave for hydrothermal treatment, together with a mixed solution of 15 mL of H_2O_2, 0.3 g of melamine, and HNO_3, and kept for 72 h at a temperature of 80 °C. After hydrothermal treatment, the Ti-TiO_2(NW) electrode was washed, dried in a vacuum, and treated in the oven at 500 °C for 4 h.

II. Preparation of the Ti-TiO_2(NW)/rGO hybrid electrode: The second stage obtaining of the Ti-TiO_2(NW)/rGO hybrid electrode is supposed to be the deposition of rGO on the Ti-TiO_2(NW) electrode using the spin-coating method. To obtain a Ti-TiO_2(NW)/rGO

hybrid electrode, 4 mL of GO was ultra-sounded for 10 min and deposited by a facile and effective spin coating (WS-400-6NPPB Spin Coater-Laurell Technology Corporation, Lansdale, PA, USA) methodology using 1500 rot for 20 sec, which was repeated three times on both sides of Ti-TiO_2(NW) electrode. After each layer, the electrode was dried at 60 °C for 20 min and finally was applied a thermal treatment in a tubular furnace (GSL1100X Tube Furnace Vacuum System, MTI Corporation, Richmond, CA, USA) in a controlled atmosphere of nitrogen flow (80 mL min^{-1}) at a temperature of 500 °C for 4 h.

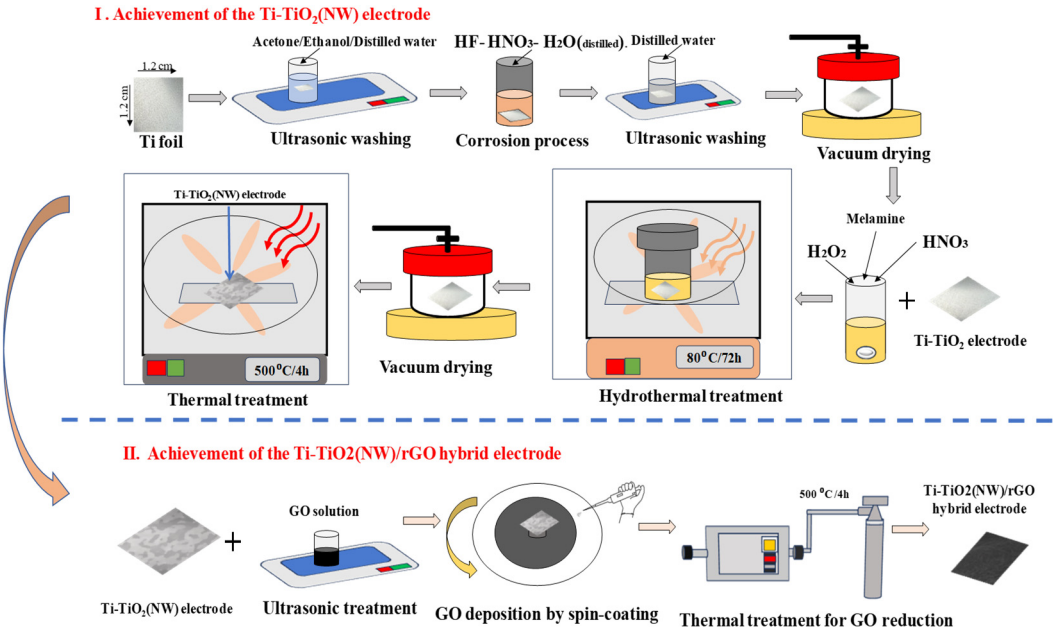


Figure 9. The schematic representation of the development of the Ti-TiO_2(NW)/rGO hybrid electrode.

3.3. Characterization Methods of the Ti-TiO_2(NW)/rGO Electrode

The morphology of the Ti-TiO_2(NW)/rGO electrode was analyzed through scanning electron microscopy (SEM, FEI Inspect S model, Eindhoven, The Netherlands) coupled with the energy dispersive X-ray analysis detector (EDX) for elemental analysis and to examine the optical characteristics of the hybrid material, UV-visible spectroscopy (PerkinElmer Lambda 950 UV/Vis spectrophotometer, Shelton, CT, USA) equipped with an integrating sphere in the range of 400–600 nm was used. The crystalline structure of the electrode was characterized using X-ray diffraction (XRD, PANalytical X'Pert PRO MPD Diffractometer, Almelo, The Netherlands) with Cu-Kα radiation in the range 2θ = 10–80°. The vibrational states of the electrode were identified by Raman spectroscopy with a Nanonics Imaging (Jerusalem, Israel)—MultiProbe Imaging—MultiView 1000™Platform (SPM).

The electrochemical characterization was performed by cyclic voltammetry using an Autolab potentiostat/galvanostat (PGSTAT 302 MetrohmAutolab B.V., Utrecht, The Netherlands) controlled with GPES 4.9 software using a three-electrode cell system in a 1 M KNO_3 solution, where Ti/TiO_2(NW)/rGO (an effective area of 0.5 cm^2) acted as working electrodes, Ag/AgCl served as the reference electrode, and platinum plate acted as the counter electrode.

4. Conclusions

In this research, a hybrid electrode based on a Ti-TiO_2(NW)/rGO structure was successfully achieved in two stages, using hydrothermal treatment followed by spin-coating deposition methodology. The hybrid electrode was structurally, morphologically, and electrochemically characterized by specific methods and tested in electrooxidation and

photo-electrooxidation processes of doxorubicin emergent pollutants. Thus, structural analysis by XRD spectra confirmed the successful formation of all three polymorphic phases of TiO_2 at lower temperatures compared to other studies, highlighting the potential for further improvements in TiO_2 nanowires synthesized using a melamine template. Additionally, the broad intensity peak at 2theta = 20–30°, corresponding to the (002) plane of rGO, confirms the reduction of GO to rGO. The reduction of GO is also confirmed by the Raman spectroscopy by the ratio of I_D/I_G peaks about 1.15. The SEM micrographs indicate that the surface of the titanium foil was preferentially corroded, favoring the formation of channels on the surface, and the TiO_2 nanowires showed a random growth on the islands on the electrode surface, and the uniform deposition of rGO on the electrode surface is evidenced. In conclusion, this study successfully developed a new and effective electrode material that can be applied for the degradation of DOX by both electrooxidation and photo-electrooxidation processes. The presence of chloride acts as a supplementary oxidant besides hydroxyl radicals, which enhances DOX degradation. Under UV irradiation and the 7 V/SCE applied potential in the photo-electrooxidation process, a degradation rate of about 80% after 90 min for a concentration of 2.5 mg L^{-1} DOX was obtained. Moreover, the facile synthesis of the Ti-TiO_2(NW)/rGO electrode, as well as the high-efficiency rate of DOX during the photo-electrooxidation process, opens new perspectives for other emerging compounds from water.

Author Contributions: Conceptualization, M.-I.M., C.L. and C.B.; methodology, M.-I.M., C.B., C.O. and C.L.; validation C.B. and N.D.; investigation, M.-I.M., M.N. and C.O; writing—original draft preparation, M.-I.M., M.N., C.O., C.L, C.B. and N.D.; writing—review and editing, M.-I.M., C.O., C.L, C.B. and N.D.; visualization, C.B. and N.D.; supervision, C.L., N.D. and C.B. All authors have read and agreed to the published version of the manuscript.

Funding: This research was funded by a grant from the Ministry of Research, Innovation, and Digitization, project number PN-IV-P8-8.3-ROMD-2023-0227 within PNCDI IV, and partially by the project code PN 23 27 01 02 INOMAT, 23-27 29N/2023.

Institutional Review Board Statement: Not applicable.

Informed Consent Statement: Not applicable.

Data Availability Statement: The original contributions presented in this study are included in the article. Further inquiries can be directed to the corresponding authors.

Conflicts of Interest: The authors declare no conflicts of interest.

References

1. Festinger, N.; Kisielewska, A.; Burnat, B.; Ranoszek-Soliwoda, K.; Grobelny, J.; Koszelska, K.; Guziejewski, D.; Smarzewska, S. The Influence of Graphene Oxide Composition on Properties of Surface-Modified Metal Electrodes. *Materials* **2022**, *15*, 7684. [CrossRef] [PubMed]
2. Kumar, S. Synthesis of reduced graphene oxide (rGO) via chemical reduction. *AIP Conf. Proc.* **2015**, *1661*, 080032. [CrossRef]
3. Hidayat, R.; Wahyuningsih, S.; Ramelan, A. Simple synthesis of rGO (reduced graphene oxide) by thermal reduction of GO (graphene oxide). *IOP Conf. Ser. Mater. Sci. Eng.* **2020**, *858*, 012009. [CrossRef]
4. Quezada Renteria, A.; Ruiz-Garcia, C.; Sauvage, T.; Chazaro-Ruiz, L.; Rangel-Mendez, J.; Ania, C. Photochemical and electrochemical reduction of graphene oxide thin films: Tuning the nature of surface defects. *Phys. Chem. Chem. Phys. PCCP* **2020**, *22*, 20732–20743. [CrossRef]
5. Vinodgopal, K.; Neppolian, B.; Lightcap, I.; Grieser, F.; Ashokkumar, M.; Kamat, P. Sonolytic Design of Graphene−Au Nanocomposites. Simultaneous and Sequential Reduction of Graphene Oxide and Au(III). *J. Phys. Chem. Lett.* **2010**, *1*, 1987–1993. [CrossRef]
6. Bonando, M.G.; Mór Moreira, G.M.; Moraes Fernandes, N.M.; Steinberg, D.; Cadore, A.R.; de Carvalho Castro Silva, C.; Miyazato Saito, L.A. The impact of different flexible substrates on the photothermal reduction quality of graphene oxide. *Nanoscale Adv.* **2024**, *6*, 4604–4610. [CrossRef]

7. Xie, X.; Zhou, Y.; Huang, K. Advances in Microwave-Assisted Production of Reduced Graphene Oxide. *Front. Chem.* **2019**, *7*, 355. [CrossRef]
8. Xie, G.; Forslund, M.; Pan, J. Direct Electrochemical Synthesis of Reduced Graphene Oxide (rGO)/Copper Composite Films and Their Electrical/Electroactive Properties. *ACS Appl. Mater. Interfaces* **2014**, *6*, 7444–7455. [CrossRef]
9. Amalraj, M.; John, S.A. *Graphene-Modified Electrochemical Sensors*; Elsevier: Amsterdam, The Netherlands, 2019; pp. 1–41.
10. Kumar, M.; Mangalam, J. High absorptivity and visible light assisted photocatalytic activity of silver/reduced graphene oxide (Ag/rGO) nanocomposite for wastewater treatment. *Nano-Struct. Nano-Objects* **2018**, *17*, 58–66. [CrossRef]
11. Liu, Y. Hydrothermal synthesis of TiO_2–RGO composites and their improved photocatalytic activity in visible light. *RSC Adv.* **2014**, *4*, 36040–36045. [CrossRef]
12. Sun, N.; Ma, J.; Wang, C.; Xue, J.; Qiang, L.; Tang, J. A facile and efficient method to directly synthesize TiO_2/rGO with enhanced photocatalytic performance. *Superlattices Microstruct.* **2018**, *121*, 1–8. [CrossRef]
13. Cho, E.-S.; Park, S.-J.; Kim, S. Synthesis of GNS/TiO_2 Electrodes Through Sol–Gel Method and Their Electrochemical Analysis for Capacitors. *J. Nanosci. Nanotechnol.* **2016**, *16*, 8594–8597. [CrossRef]
14. Guo, J.; Zhu, S.; Chen, Z.; Li, Y.; Yu, Z.; Liu, Q.; Li, J.; Feng, C.; Zhang, D. Sonochemical synthesis of TiO_2 nanoparticles on graphene for use as photocatalyst. *Ultrason. Sonochem.* **2011**, *18*, 1082–1090. [CrossRef]
15. Meng, X.; Geng, D.; Liu, J.; Li, R.; Sun, X. Controllable Synthesis of Graphene-Based Titanium Dioxide Nanocomposites by Atomic Layer Deposition. *Nanotechnology* **2011**, *22*, 165602. [CrossRef]
16. Jiang, J.; Li, Y.; Liu, J.; Huang, X.; Yuan, C.; Lou, X.W. Recent Advances in Metal Oxide-based Electrode Architecture Design for Electrochemical Energy Storage. *Adv. Mater.* **2012**, *24*, 5166–5180. [CrossRef]
17. Pratama, D.S.A.; Haryanto, A.; Lee, C.W. Heterostructured mixed metal oxide electrocatalyst for the hydrogen evolution reaction. *Front. Chem.* **2023**, *11*, 1141361. [CrossRef]
18. Sugawara, Y.; Hihara, T.; Anilkumar, G.M.; Kamata, K.; Yamaguchi, T. Metal oxide electrocatalyst support for carbon-free durable electrodes with excellent corrosion resistance at high potential conditions. *Sustain. Energy Fuels* **2021**, *5*, 1374–1378. [CrossRef]
19. Tobaldi, D.M.; Dvoranová, D.; Lajaunie, L.; Rozman, N.; Figueiredo, B.; Seabra, M.P.; Škapin, A.S.; Calvino, J.J.; Brezová, V.; Labrincha, J.A. Graphene-TiO_2 hybrids for photocatalytic aided removal of VOCs and nitrogen oxides from outdoor environment. *Chem. Eng. J.* **2021**, *405*, 126651. [CrossRef]
20. Ghasemi, S.; Esfandiar, A.; Rahman Setayesh, S.; Habibi-Yangjeh, A.; Iraji Zad, A.; Gholami, M. Synthesis and characterization of TiO_2–graphene nanocomposites modified with noble metals as a photocatalyst for degradation of pollutants. *Appl. Catal. A Gen.* **2013**, *462–463*, 82–90. [CrossRef]
21. Xin, X.; Zhou, X.; Wu, J.; Yao, X.; Liu, Z. Scalable Synthesis of TiO_2/Graphene Nanostructured Composite with High-Rate Performance for Lithium Ion Batteries. *ACS Nano* **2012**, *6*, 11035–11043. [CrossRef]
22. Cheng, P.; Yang, Z.; Wang, H.; Cheng, W.; Chen, M.; Shangguan, W. TiO_2-graphene nanocomposites for photocatalytic hydrogen production from splitting water. *Fuel Energy Abstr.* **2012**, *37*, 2224–2230. [CrossRef]
23. Cui, H.-F.; Wu, W.-W.; Li, M.-M.; Song, X.; Lv, Y.; Zhang, T.-T. A highly stable acetylcholinesterase biosensor based on chitosan-TiO_2-graphene nanocomposites for detection of organophosphate pesticides. *Biosens. Bioelectron.* **2018**, *99*, 223–229. [CrossRef] [PubMed]
24. Le, T.-L.T.; Le, T.-H.T.; Nguyen Van, K.; Van Bui, H.; Le, T.G.; Vo, V. Controlled growth of TiO_2 nanoparticles on graphene by hydrothermal method for visible-light photocatalysis. *J. Sci. Adv. Mater. Devices* **2021**, *6*, 516–527. [CrossRef]
25. Kusiak-Nejman, E.; Morawski, A.W. TiO_2/graphene-based nanocomposites for water treatment: A brief overview of charge carrier transfer, antimicrobial and photocatalytic performance. *Appl. Catal. B Environ.* **2019**, *253*, 179–186. [CrossRef]
26. Nipane, S.; Lee, S.-W.; Gokavi, G.; Kadam, A. In situ one pot synthesis of nanoscale TiO_2-anchored reduced graphene oxide (RGO) for improved photodegradation of 5-fluorouracil drug. *J. Mater. Sci. Mater. Electron.* **2018**, *29*, 16553–16564. [CrossRef]
27. Buerge, I.J.; Buser, H.-R.; Poiger, T.; Müller, M.D. Occurrence and Fate of the Cytostatic Drugs Cyclophosphamide and Ifosfamide in Wastewater and Surface Waters. *Environ. Sci. Technol.* **2006**, *40*, 7242–7250. [CrossRef]
28. Kovalova, L.; McArdell, C.S.; Hollender, J. Challenge of high polarity and low concentrations in analysis of cytostatics and metabolites in wastewater by hydrophilic interaction chromatography/tandem mass spectrometry. *J. Chromatogr. A* **2009**, *1216*, 1100–1108. [CrossRef]
29. Alsoliemy, A. Doxorubicin removal from an aqueous environment efficiently using bimetallic organic frameworks: Synthesis, characterization, and optimization of adsorption procedure using the Box–Behnken design. *J. Mol. Liq.* **2024**, *415*, 126360. [CrossRef]
30. Azuma, T.; Hayashi, T. On-site chlorination responsible for effective disinfection of wastewater from hospital. *Sci. Total Environ.* **2021**, *776*, 145951. [CrossRef]

31. Tang, K.; Spiliotopoulou, A.; Chhetri, R.K.; Ooi, G.T.H.; Kaarsholm, K.M.S.; Sundmark, K.; Florian, B.; Kragelund, C.; Bester, K.; Andersen, H.R. Removal of pharmaceuticals, toxicity and natural fluorescence through the ozonation of biologically-treated hospital wastewater, with further polishing via a suspended biofilm. *Chem. Eng. J.* **2019**, *359*, 321–330. [CrossRef]
32. Beier, S.; Köster, S.; Krebber, K.; Schröder, H.; Pinnekamp, J. Treatment of hospital wastewater effluent by nanofiltration and reverse osmosis. *Water Sci. Technol. A J. Int. Assoc. Water Pollut. Res.* **2010**, *61*, 1691–1698. [CrossRef] [PubMed]
33. Macías-García, A.; García-Sanz-Calcedo, J.; Carrasco-Amador, J.P.; Segura-Cruz, R. Adsorption of Paracetamol in Hospital Wastewater Through Activated Carbon Filters. *Sustainability* **2019**, *11*, 2672. [CrossRef]
34. Rawal, A.; Saraswat, H. Stabilisation of soil using hybrid needlepunched nonwoven geotextiles. *Geotext. Geomembr.* **2011**, *29*, 197–200. [CrossRef]
35. Ensano, B.M.B.; Borea, L.; Naddeo, V.; Belgiorno, V.; de Luna, M.D.G.; Balakrishnan, M.; Ballesteros, F.C. Applicability of the electrocoagulation process in treating real municipal wastewater containing pharmaceutical active compounds. *J. Hazard. Mater.* **2019**, *361*, 367–373. [CrossRef]
36. Baciu, A.; Orha, C.; Nicolae, R.; Nicolaescu, M.; Ilies, S.; Manea, F. Advanced Electrochemical Degradation of Organic Pollutants from Water Using Sb-Doped SnO_2/Ti Anode and Assisted by Granular Activated Carbon. *Coatings* **2023**, *13*, 1127. [CrossRef]
37. Orha, C.; Bandas, C.; Lazau, C.; Popescu, M.I.; Baciu, A.; Manea, F. Advanced Electrodegradation of Doxorubicin in Water Using a 3-D Ti/SnO_2 Anode. *Water* **2022**, *14*, 821. [CrossRef]
38. Bandas, C.; Popescu, M.I.; Orha, C.; Nicolaescu, M.; Pop, A.; Lazau, C. Development of Hybrid Electrodes Based on a Ti/TiO_2 Mesoporous/Reduced Graphene Oxide Structure for Enhanced Electrochemical Applications. *Coatings* **2023**, *13*, 1359. [CrossRef]
39. Holzwarth, U.; Gibson, N. The Scherrer equation versus the 'Debye-Scherrer equation'. *Nat. Nanotechnol.* **2011**, *6*, 534. [CrossRef]
40. Yu, Y.; Wen, W.; Qian, X.-Y.; Liu, J.-B.; Wu, J.-M. UV and visible light photocatalytic activity of Au/TiO_2 nanoforests with Anatase/Rutile phase junctions and controlled Au locations. *Sci. Rep.* **2017**, *7*, 41253. [CrossRef]
41. Guo, W.; Li, Y.; Tang, Y.; Chen, S.; Liu, Z.; Wang, L.; Zhao, Y.; Gao, F. TiO_2 Nanowire Arrays on Titanium Substrate as a Novel Binder-free Negative Electrode for Asymmetric Supercapacitor. *Electrochim. Acta* **2017**, *229*, 197–207. [CrossRef]
42. Mikhaylov, P.; Vinogradov, M.; Levin, I.; Shandryuk, G.; Lubenchenko, A.; Kulichikhin, V. Synthesis and characterization of polyethylene terephthalate-reduced graphene oxide composites. *IOP Conf. Ser. Mater. Sci. Eng.* **2019**, *693*, 012036. [CrossRef]
43. Sheshmani, S.; Nayebi, M. Modification of TiO_2 with graphene oxide and reduced graphene oxide; enhancing photocatalytic activity of TiO_2 for removal of remazol Black B. *Polym. Compos.* **2017**, *40*, 210–216. [CrossRef]
44. Makuła, P.; Pacia, M.; Macyk, W. How To Correctly Determine the Band Gap Energy of Modified Semiconductor Photocatalysts Based on UV–Vis Spectra. *J. Phys. Chem. Lett.* **2018**, *9*, 6814–6817. [CrossRef] [PubMed]
45. González-Meza, O.; Larios-Durán, E.R.; Gutierrez-Becerra, A.; Casillas, N.; Escalante, J.; Barcena-Soto, M. Development of a Randles-Ševčík-like equation to predict the peak current of cyclic voltammetry for solid metal hexacyanoferrates. *J. Solid State Electrochem.* **2019**, *23*, 3123–3133. [CrossRef]
46. Konopka, S.J.; McDuffie, B. Diffusion coefficients of ferri- and ferrocyanide ions in aqueous media, using twin-electrode thin-layer electrochemistry. *Anal. Chem.* **1970**, *42*, 1741–1746. [CrossRef]
47. Salazar, C.; Contreras, N.; Mansilla, H.D.; Yáñez, J.; Salazar, R. Electrochemical degradation of the antihypertensive losartan in aqueous medium by electro-oxidation with boron-doped diamond electrode. *J. Hazard. Mater.* **2016**, *319*, 84–92. [CrossRef]
48. Ferreira Garcia, L.; Gonçalves Moreno, E.K.; Barroso Brito, L.; Rodrigues de Oliveira, G.A.; Linares, J.J.; de Souza Gil, E. Effective degradation of the antineoplastic doxorubicin by electrochemical oxidation on boron doped diamond. *J. Electroanal. Chem.* **2020**, *870*, 114252. [CrossRef]
49. Yue, H.Y.; Guan, E.H.; Gao, X.; Yao, F.; Wang, W.Q.; Zhang, T.; Wang, Z.; Song, S.S.; Zhang, H.J. Hydrothermal Synthesis of TiO_2 Nanowires-Reduced Graphene Oxide Nanocomposite to Enhance Electrochemical Performance in Supercapacitor. *ChemistrySelect* **2018**, *3*, 12455–12460. [CrossRef]
50. Moreno, E.K.G.; Garcia, L.F.; Lobón, G.S.; Brito, L.B.; Oliveira, G.A.R.; Luque, R.; de Souza Gil, E. Ecotoxicological assessment and electrochemical remediation of doxorubicin. *Ecotoxicol. Environ. Saf.* **2019**, *179*, 143–150. [CrossRef]
51. Racles, C.; Zaltariov, M.-F.; Silion, M.; Macsim, A.-M.; Cozan, V. Photo-oxidative degradation of doxorubicin with siloxane MOFs by exposure to daylight. *Environ. Sci. Pollut. Res.* **2019**, *26*, 19684–19696. [CrossRef]
52. Abbasi, M.A.; Amin, K.M.; Ali, M.; Ali, Z.; Atif, M.; Ensinger, W.; Khalid, W. Synergetic effect of adsorption-photocatalysis by GO−CeO_2 nanocomposites for photodegradation of doxorubicin. *J. Environ. Chem. Eng.* **2022**, *10*, 107078. [CrossRef]
53. Wood, M.J.; Irwin, W.J.; Scott, D.K. Photodegradation of Doxorubicin, Daunorubicin and Epirubicin Measured by High-Performance Liquid Chromatography. *J. Clin. Pharm. Ther.* **1990**, *15*, 291–300. [CrossRef] [PubMed]
54. Kadu, B.S.; Wani, K.D.; Kaul-Ghanekar, R.; Chikate, R.C. Degradation of doxorubicin to non-toxic metabolites using Fe-Ni bimetallic nanoparticles. *Chem. Eng. J.* **2017**, *325*, 715–724. [CrossRef]

55. Dumitru, R.; Ianculescu, A.; Păcurariu, C.; Lupa, L.; Pop, A.; Vasile, B.; Surdu, A.; Manea, F. $BiFeO_3$-synthesis, characterization and its photocatalytic activity towards doxorubicin degradation from water. *Ceram. Int.* **2019**, *45*, 2789–2802. [CrossRef]
56. Gil, E.; Moreno, E.; Garcia, L.; Linares Leon, J. Performance Evaluation of Active and Non-active Electrodes for Doxorubicin Electro-oxidation. *KnE Eng.* **2020**, 1–9. [CrossRef]

Disclaimer/Publisher's Note: The statements, opinions and data contained in all publications are solely those of the individual author(s) and contributor(s) and not of MDPI and/or the editor(s). MDPI and/or the editor(s) disclaim responsibility for any injury to people or property resulting from any ideas, methods, instructions or products referred to in the content.